Atmos. Chem. Phys. Discuss., doi:10.5194/acp-2016-1109, 2016
Manuscript under review for journal Atmos. Chem. Phys.
Published: 14 December 2016

Atmospheric Chemistry and Physics Discussions

Is increasing ice crystal sedimentation velocity in geoengineering simulations a good proxy for cirrus cloud seeding?

Blaž Gasparini[1], Steffen Münch[1], Laure Poncet[1], Monika Feldmann[1], and Ulrike Lohmann[1]
[1]Institute for Atmospheric and Climate Science, ETH Zürich
Correspondence to: Blaž Gasparini (blaz.gasparini@env.ethz.ch)

Abstract. The complex microphysical details of cirrus seeding with ice nucleating particles (INP) in numerical simulations are often mimicked by increasing ice crystal sedimentation velocities. So far it has not been tested whether these results are comparable to geoengineering simulations in which cirrus clouds are seeded with INP. We compare simulations where the ice crystal sedimentation velocity is increased at temperatures colder than -35°C with simulations of cirrus seeding with INP using the ECHAM-HAM general circulation model. The radiative flux response of the two methods shows a similar behaviour in terms of annual and seasonal averages. Both methods decrease surface temperature but increase precipitation in response to a decreased atmospheric stability. Moreover, simulations of seeding with INP lead to a decrease in liquid clouds, which counteracts part of the cooling due to changes in cirrus clouds. The liquid cloud response is largely avoided in a simulation where seeding occurs during night only. Simulations with increased ice crystal sedimentation velocity, on the contrary, lead to counteracting mixed-phase cloud responses. The increased sedimentation velocity simulations induce a 30% larger surface temperature response, due to their lower altitude of maximum diabatic forcing compared with simulations of seeding with INP particles. They can counteract up to 60% of the radiative effect of CO_2 doubling with a maximum net top-of-the-atmosphere forcing of -2.2 W m^{-2}.

1 Introduction

Cirrus seeding is a proposed geoengineering method to decrease the occurrence of cirrus clouds by changing their optical properties to increase the amount of outgoing longwave (LW) radiation (Mitchell and Finnegan, 2009) and thereby cooling the climate. Cirrus clouds on average have a stronger LW than shortwave (SW) effect on the radiative balance, leading to a positive net cloud radiative effect (CRE), as estimated from satellite data (Hartmann et al., 1992; Chen et al., 2000; Futyan et al., 2005; Hong et al., 2016), in situ lidar observations (Kienast-Sjögren et al., 2016), and global modelling studies (Gasparini and Lohmann, 2016). Cirrus CRE has a pronounced seasonal and daily cycle, with higher values in the winter hemisphere (or at night) where the reflection of SW radiation is limited by the lack of insolation. We define cirrus clouds as all clouds that form at temperatures lower than -35°C with no additional altitude criteria.

Two microphysical formation pathways of cirrus clouds exist:

Atmos. Chem. Phys. Discuss., doi:10.5194/acp-2016-1109, 2016
Manuscript under review for journal Atmos. Chem. Phys.
Published: 14 December 2016

Atmospheric Chemistry and Physics Discussions

- Homogeneous freezing of solution droplets occurs at high relative humidities with respect to ice (RH_{ice}) and can lead to a large number of ice crystals (IC) depending on temperature, updraft velocity, and relative humidity with respect to ice (Kärcher and Lohmann, 2002). If their concentration is large, their growth is limited, as they rapidly consume the available water vapour (Ickes et al., 2015).

- Heterogeneous freezing can occur in the presence of effective ice nucleating particles (INP) which lowers the freezing energy barrier, allowing droplets to freeze at lower RH_{ice} and/or smaller updraft velocities (Kärcher and Ström, 2003; Hoose and Möhler, 2012).

Heterogeneous ice nucleation can suppress homogeneous nucleation in conditions of slow updrafts, commonly found in the upper troposphere (Jensen et al., 2016; Kärcher and Ström, 2003), resulting in optically thinner and shorter-lived cirrus clouds. A modelling study by Lohmann et al. (2008) showed that the global net top-of-the-atmosphere (TOA) radiative balance can change by up to 2.8 $W\,m^{-2}$ as a result of a complete shift from homogeneous to heterogeneous cirrus formation (the numbers are reported in Mitchell and Finnegan (2009)). As the upper tropospheric INP number concentrations are limited (DeMott et al., 2003), only few IC can nucleate heterogeneously and consequently grow to larger sizes (Kuebbeler et al., 2014).

A large fraction of cirrus clouds at temperatures warmer than -60°C is found to have formed from homogeneous nucleation of cloud droplets in the convective clouds forming anvil cirrus clouds (Jensen et al., 2015). These cannot be modified by seeding of INP as their formation is dominated by the dynamics (Penner et al., 2015). In addition, IC in warm cirrus in the extratropics often form by freezing of cloud droplets in mixed-phase clouds, which are subsequently advected to cirrus conditions (Luebke et al., 2016; Wernli et al., 2016; Voigt et al., 2016). Cirrus seeding can perturb only the nucleation and initial growth processes and therefore cannot influence the IC that nucleated at temperatures between 0°C and -35°C in the mixed-phase clouds.

Cirrus seeding tries to modify the competition between homogeneously and heterogeneously formed IC by artificial injections of efficient INP with the goal of cooling the climate. Modelling studies by Storelvmo and Herger (2014) and Storelvmo et al. (2014) suggested that cirrus seeding can decrease the net TOA radiative balance by up to 2 $W\,m^{-2}$ or decrease the surface temperature by up to 1.4 °C. On the other hand, a study by Penner et al. (2015) showed no significant net radiative change as a result of seeding due to a larger concentration of upper tropospheric INP in their reference climate, no upper limit on the subgrid-scale updraft velocities, and the inclusion of the competition of pre-existing IC for the available water vapour. Gasparini and Lohmann (2016) also found an insignificant radiative response to cirrus seeding in their simulations. They attributed it to a decrease in IC radius and an increase in cirrus cloud cover by forming new cirrus in previously cloud free ice supersaturated regions.

As it is computationally demanding to simulate the detailed cirrus microphysical processes, climatic responses of seeding are often represented by increasing the IC sedimentation velocity in cirrus clouds (Muri et al., 2014; Crook et al., 2015; Jackson et al., 2016). Increasing the IC sedimentation velocity can, analogous to seeding, decrease the amount of cirrus cloud cover,

Atmos. Chem. Phys. Discuss., doi:10.5194/acp-2016-1109, 2016
Manuscript under review for journal Atmos. Chem. Phys.
Published: 14 December 2016

Atmospheric Chemistry and Physics Discussions

ice water content (IWC), and ice crystal number concentration (ICNC). Such a modelling strategy was also selected by the Geoengineering Modeling Intercomparison Project (Kravitz et al., 2015). However, it has never been systematically analysed whether this method leads to results comparable to seeding with INP.

In this paper we compare the radiative, microphysical, and climatic responses between the increased sedimentation velocity and seeding simulations with the help of suitable INP. We point out differences between the two setups, examine liquid and mixed-phase cloud responses to changes in cirrus clouds, and show geographical areas where both ways of simulating cirrus geoengineering are most effective. We also evaluate the maximum effect of the increased sedimentation velocity schemes.

2 Methods

2.1 Model setup

We use the ECHAM6-HAM2 aerosol-climate model (Stevens et al., 2013; Zhang et al., 2012; Neubauer et al., 2014) with a horizontal resolution of 1.875° × 1.875° and 31 vertical levels. The model top is at 10 hPa. The level thickness at typical cirrus altitudes varies between 500 and 1000 m. The two moment aerosol scheme (Vignati et al., 2004; Stier et al., 2005) interactively simulates aerosol emissions, their growth, coagulation and sink processes in terms of their number and mass mixing ratios. The model uses a two moment microphysics cloud scheme (Lohmann et al., 2007) with prognostic equations for cloud liquid and ice mass mixing ratios as well as cloud droplet and ice crystal number concentrations. The cirrus nucleation scheme by Kärcher et al. (2006) simulates the competition between homogeneous freezing, heterogeneous freezing, and deposition of water vapour on pre-existing IC. Heterogeneous freezing occurs via deposition nucleation of insoluble coarse and accumulation mode dust aerosols or immersion freezing of internally mixed (coated) dust aerosols based on laboratory measurements by Möhler et al. (2006, 2008). The detailed implementation of the cirrus formation scheme in the ECHAM-HAM general circulation model has been described in Kuebbeler et al. (2014) and Gasparini and Lohmann (2016).
We use the convective mass flux scheme of Tiedtke (1989) with modifications for deep convection from Nordeng (1994), which is an important source of detrained cloud ice leading to frequent anvil cirrus formation.

2.2 Experimental setup

For the idealized seeding scenario we perform simulations where the sedimentation velocity of all IC at temperatures below -35°C is increased by a factor of 2 (simulation VEL2), 4 (VEL4), and 8 (VEL8), and two simulations where the sedimentation velocity is either always set to 2 m s^{-1} (VELmax) or only during night (VELmaxN). 2 m s^{-1} is the maximum sedimentation velocity IC can achieve in our model. We always show anomalies with respect to the reference, unperturbed simulation (REF). Fig. 1 shows the relation of IC size and their sedimentation velocity following the formulation by Spichtinger and Gierens (2009) for typical upper tropospheric conditions in the tropics. The upper sedimentation velocity limit of 2 m s^{-1} used in ECHAM-HAM does not significantly influence our results, as IC with a radius smaller than 90 μm in atmospherically relevant

Atmos. Chem. Phys. Discuss., doi:10.5194/acp-2016-1109, 2016
Manuscript under review for journal Atmos. Chem. Phys.
Published: 14 December 2016

Atmospheric Chemistry and Physics Discussions

conditions do not sediment faster than approximately 0.3 m s^{-1}. Ice crystals larger than 90 μm are transferred from ice into snow (Levkov et al., 1992) and precipitate out of the atmosphere within one model timestep.

For the realistic seeding scenarios, we performed 5 simulations of globally uniform continuous seeding in areas with temperature colder than -35°C as decribed by Gasparini and Lohmann (2016). In SEED we use INP with the modal radius of 0.5 μm, while in SEEDr50 the radius is increased to 50 μm. In this way we overcame the problem of a cloud cover increase and IC radius decrease that we see when seeding with 0.5 μm particles (Gasparini and Lohmann, 2016). We do not go beyond a radius of 50 μm despite using even larger INP sizes would likely result in larger climatic impacts; as the injected particle mass increases cubically with particle size, its practical use will be limited due to the needed delivery into the upper troposphere and shorter atmospheric residence time. We seed all areas supersaturated with respect to ice at temperatures below -35°C with 0.1, 0.3, 1, 3, 10, 30, and 100 INP L^{-1} (consequently we name the simulations as SEED0.1r50, SEED0.3r50, SEED1r50, etc., Table 1), which freeze at RH_{ice} as low as 105% (Mitchell and Finnegan, 2009). In addition, we simulate a scenario where seeding with large INP is applied only during night (SEED1r50N). It is important to note that we only modify in situ formed cirrus and not the convective anvil clouds. Furthermore, the injected INP do not interact with radiation and cannot influence mixed-phase or liquid clouds.

All simulations are run for 5 years with fixed sea surface temperatures (SST) to study radiative flux anomalies and fast responses to seeding. Simulations SEED1r50 and VEL2 are extended to 10 years to increase the statistical robustness of the results. They are additionally simulated in the mixed layer ocean (MLO) setup in order to study long term microphysical and climatic responses, especially temperture and precipiation. The MLO simulations are run for 50 years, but we only assess the anomalies of the last 30 simulated years, after the model has reached an equilibrium. A list of all simulations and their specifications can be found in the Table 1. The significance is calculated based on a double-sided Welch's t-test at the 95% significance level.

3 Results

3.1 Cirrus geoengineering

3.1.1 Increased sedimentation velocity

The radiative effects decrease exponentially with the increase in sedimentation velocity (Fig. 2a) as already noted by Jackson et al. (2016). This is because the cirrus CRE always decreases for about 30% when doubling the IC sedimentation velocity, i.e. comparing REF and VEL2, VEL2 and VEL4, or VEL4 and VEL8 (Table 2). In the VELmax simulation increasing IC sedimentation velocities in cirrus to 2 m s^{-1} leads to a negative net TOA radiative balance anomaly of -2.20 W m^{-2} $\pm$ 0.26 W m^{-2} which corresponds to about 60% of the radiative forcing induced by the doubling of the CO_2 concentrations (Stocker,

Atmos. Chem. Phys. Discuss., doi:10.5194/acp-2016-1109, 2016
Manuscript under review for journal Atmos. Chem. Phys.
Published: 14 December 2016

Atmospheric Chemistry and Physics Discussions

T.F., D. Qin, G.-K. Plattner, L.V. Alexander, S.K. Allen, N.L. Bindoff, F.-M. Bréon, J.A. Church et al., 2013).

In VELmaxN we only increase the IC sedimentation velocity in cirrus during night, which leads to an overall (considering day and night) 15-20% smaller radiative effect decrease. The result is consistent with the cirrus CRE diurnal cycle diagnosed from the model, which reaches 8 W m^{-2} in the global annual average at night and 1 W m^{-2} during day, when cirrus reflect part of the incoming SW radiation. Even though the fall velocity in the VELmax simulation corresponds to an unrealistically large IC at typical cirrus levels (Fig. 1), the simulation shows that globally uniform cirrus cloud thinning cannot reduce the cirrus CRE by more than ∼50% (Table 3).

3.1.2 Cirrus seeding with ice nucleating particles

In the SEED simulations we inject seeding INP of 0.5 μm radius at every model timestep in areas with temperatures colder than -35°C. We see no significant radiative response for concentrations of up to 1 INP L^{-1} (Fig. 2b), while a net TOA positive radiative anomaly develops for seeding with more than 3 INP L^{-1} (overseeding) as explained in detail in Gasparini and Lohmann (2016). With an increased radius of 20 and 50 μm (simulations SEEDr20 and SEEDr50) and a seeding concentration of 1 INP L^{-1}, we achieve a significant negative TOA radiative anomaly of -0.46 ± 0.14 W m^{-2} and -0.85 ± 0.40 W m^{-2}, respectively (Fig. 2c and Table 4). Seeding with large INP particles leads to larger newly formed heterogeneous IC and therefore avoids their decrease in size as observed in Gasparini and Lohmann (2016). Moreover, the initial increase in cloud cover by seeding of ice supersaturated clear sky regions with very efficient INP particles is outweighted by the large increase in the IC sedimentation velocities, which leads to a net cirrus cloud cover decrease (Fig. 4a).

Large INP have a shorter atmospheric lifetime because of the quadratic dependence of particle fallspeed on its radius where the impact of turbulence can be neglected as we are in Stokes regime. For instance, the vertical velocity of a 0.5 μm aerosol particle (considering a density of 2500 kg m^{-3}, similar to dust aerosols) in the upper troposphere is $\sim 10^{-4}$ m s^{-1}, while a 50 μm particle falls with a velocity of 1 m s^{-1}. On the other hand, the freezing probability P as described by the classical nucleation theory (Eq. 1), remains roughly similar, because it depends on the INP's surface area A which increases quadratically with particle size. We consider a constant nucleation rate J where Δt represents the time a particle spends in conditions favourable for freezing:

$$P = 1 - e^{-JA\Delta t} \tag{1}$$

The large size of seeding INP increases the deposition flux of water vapour onto the INP leading to a more effective drying of the upper atmosphere. The largest disadvantage of seeding with large INP is the cubic dependence of particle mass on its radius: an increase in radius from 0.5 to 50 μm increases its mass by a factor of 10^6, making the transport of the seeding material to the upper troposphere much more challenging. Additionally, the seeding frequency of the large INP would probably need to

Atmos. Chem. Phys. Discuss., doi:10.5194/acp-2016-1109, 2016
Manuscript under review for journal Atmos. Chem. Phys.
Published: 14 December 2016

Atmospheric Chemistry and Physics Discussions

be larger compared with the small INP seeding, due to their faster sedimentation.

The radiative anomalies obtained by injecting 0.3 or 3 INP L^{-1} of 50 μm radius are -0.66 $\pm$ 0.35 W m^{-2} and -0.77 $\pm$ 0.27 W m^{-2} and thus not significantly different from those with 1 INP L^{-1} (Fig. 2b). The effective seeding range thus spans over about an order of magnitude of INP concentrations. The response from a simulation with large particle seeding at night only (SEED1r50N) with a net TOA radiative anomaly of -0.91 W m^{-2} is similar to the one from SEED1r50.

3.2 Response comparison

3.2.1 Radiative and microphysical responses

We now focus on the climatic and microphysical responses of the seeding with 1 INP L^{-1} (SEED1r50) and increased sedimentation velocity (VEL2) scenarios due to their similar TOA net radiative flux anomalies ($\sim$ -0.8 W m^{-2}, Fig. 3a) in 10-year fixed SST simulations. Both geoengineering simulations show a positive anomaly in net SW TOA fluxes, due to a smaller SW CRE, i.e. less SW radiation reflected by cirrus clouds. The LW radiation budget, on the other hand, is more negative due to the increased outgoing LW radiation in response to a decrease in cirrus cloud cover. The radiative changes result in increased tropospheric cooling, decreasing the atmospheric stability, increasing convection, and leading to a precipitation increase of about 1% for both VEL2 and SEED1r50 (Fig. 3b).

Interestingly, the simulation SEED1r50N leads to a slightly larger net TOA radiative anomaly, which is different from the comparison of VELmaxN and VELmax simulations and counterintuitive as the cirrus cloud radiative effects (cCRE) in ECHAM-HAM on average is positive also during the day. However, while the impact of increasing the sedimentation velocity only during night ceases immediately when the sun appears above the horizon, the seeding of INP particles can have some inertia. The effective cirrus cloud lifetime is in the range of a couple of hours as diagnosed from our model; we therefore expect the seeded clouds to prevent the formation of homogeneous cirrus also some hours after sunrise, when the sun is low on the horizon and the cirrus LW warming effect significantly outweighs the cooling by the scattering of the SW radiation. Moreover, the SEED1r50N avoids the warming effect induced by a response of liquid clouds to seeding during the day, as described in the Sect. 3.2.2.

From now on we focus only on the 30-year MLO simulation anomalies. The surface temperature decrease in response to changes in the atmosphere results in a more stable lower troposphere compared with fixed SST simulations. This overcompensates the fast (surface temperature independent) precipitation response in Fig. 3b, leading to a small decrease in global average precipitation for both scenarios (Fig. 3d).

Atmos. Chem. Phys. Discuss., doi:10.5194/acp-2016-1109, 2016
Manuscript under review for journal Atmos. Chem. Phys.
Published: 14 December 2016

Atmospheric Chemistry and Physics Discussions

Cirrus cloud cover decreases in both simulations (Fig. 4 a,b) with maximum anomalies between 7 (extratropics) and 15 km (tropics) altitude. The maximum decrease occurs at about 11 km altitude amounting to 4% in SEED1r50, whereas the decrease is about 3-4 times smaller in the VEL2 scenario (Fig. 4e). Both simulations show an IWC anomaly of about -0.2 to -0.5 mg kg^{-1} in the upper troposphere, corresponding to about 20-50% of the total IWC there (Fig. 4 k,l,o). However, the IWC decrease in VEL2 is followed by an increase of IWC of a similar magnitude in the mixed-phase cloud regime at temperatures warmer than -35°C, where the IC sedimentation velocity is restored to the reference value.

The pattern in VEL2 is a result of an unrealistic redistribution of ice mass to lower levels, while in SEED1r50 the large, newly formed IC quickly precipitate and are removed from the atmosphere. Therefore, the ice water path (IWP) decreases by about 7% in SEEDr50 but only by about 1.5% in the VEL2 simulation (Fig. 3e). In SEED1r50 the effect of quickly sedimenting large IC from cirrus levels affects also part of the IC in mixed-phase clouds, leading to a small IWC decrease also at temperatures warmer than -35°C (Fig. 4k). On the other hand, the IWC in mixed-phase clouds increases in VEL2, leading to a mixed-phase cloud glaciation effect, which is responsible for the total liquid water path decrease by about 3% and the cloud droplet number concentration (CDNC) drop by 1% (Fig. 3e and Fig. 5b).

The decrease in cirrus cloud cover changes the atmospheric diabatic heating, leading to an upper tropospheric cold anomaly of about 1°C in both simulations (Fig. 4 p,q,t). Interestingly, the location of the maximum anomaly and its vertical extent differ significantly between SEED1r50 and VEL2. The peak temperature decrease in SEED1r50 is concentrated in the tropical tropopause region, while VEL2 shows an elongated temperature decrease anomaly extending to about 7 km altitude. The reason for this 5 km difference in the altitude of peak cooling is most likely related to the inability of seeding to influence the convectively formed and other liquid origin cirrus clouds, which dominate at temperatures warmer than -50°C (Voigt et al., 2016). On the contrary in VEL2 all cirrus IC sediment regardless of their origin. Considerably larger TOA SW and LW radiative flux anomalies in SEED1r50 compared to VEL2 also indicate a higher altitude of the maximum radiative forcing anomaly in SEED1r50 (Fig. 3c). Moreover, in SEED1r50 the destabilisation of the upper troposphere leads to increased vertical velocities and increased tropical tropopause and stratospheric specific humidities. That implies higher cooling rates dominated by the LW emissivity of water vapour (Clough and Iacono, 1995), and explains part of the tropical tropopause and the stratospheric temperature signal.

3.2.2 Other cloud responses to seeding

The anomalies of cCRE are almost a factor of two larger than the net TOA balance anomalies (Fig. 2) or net TOA CRE anomalies (Fig. 3) as evaluated from the fixed SST setup, where the TOA radiative fluxes do not reach a new equilibrium. The additional diagnostics of liquid and mixed-phase CRE (Table 5) point at additional cloud responses to cirrus geoengineering that exert a positive radiative forcing. We note that the additional CRE decomposition is performed in fixed SST simulation setup which, however, leads to very similar cloud responses as in the corresponding MLO simulations.

Atmos. Chem. Phys. Discuss., doi:10.5194/acp-2016-1109, 2016
Manuscript under review for journal Atmos. Chem. Phys.
Published: 14 December 2016

Atmospheric Chemistry and Physics Discussions

The VEL2 simulation leads to a redistribution of ice from the cirrus to the lower lying mixed-phase regime, exerting a positive mixed-phase cloud forcing of about 0.5 W m^{-2} (Fig. 4l and Table 5). Changes in vertical stability most likely lead to an increase in midlevel convection and the redistribution of ice. These changes are responsible for the increases in ICNC due to detrainment (Fig. 3e). The positive anomaly in RH at 5-10 km (Fig. 4g) is concentrated in and just above areas of vertical velocity increase (not shown), driven by changes in vertical temperature gradients (Fig. 4t).

Furthermore, in SEED1r50 an increase in convective activity, expressed by an 1.2% increase in globally averaged convective precipitation, leads to a drying of the tropical planetary boundary layer and lower troposphere and a decrease in liquid cloud cover (Fig. 4a), water content and CDNC (Fig. 5 a,c and Fig. 3e). This leads to a positive liquid CRE anomaly (Table 5), similarly to what was found in studies by Rieck et al. (2012) and Sherwood et al. (2014). Interestingly, the shift from homogeneous to heterogeneous nucleation of IC leads to higher RH in the upper troposphere (Fig. 4f). The heterogeneous nucleation and growth timescale is several times longer than the homogeneous one (Köhler and Seifert, 2015), leading to slower vapour consumption by deposition on IC at our optimal seeding concentration of 1 INP L^{-1}. Moreover, the IWC in mixed-phase clouds is replaced by an increased liquid water content and a higher CDNC (Fig. 5 a,c), in particular in the extratropics, where the convective activity is less frequent.

By seeding cirrus clouds only at night (simulation SEED1r50N) we target their warming LW CRE and obtain a similar net TOA flux anomaly (-0.88 $\pm$ 0.36 W m^{-2}) without significantly perturbing the SW balance as in other simulations (Table 5). Despite obtaining a smaller annually averaged cCRE, the net radiative decrease at the TOA is similar to the one in the simulation SEED1r50 (Fig. 2c). SEED1r50N triggers only a small increase in convective activity (0.8% increase in convective precipitation compared with 2.8% in SEED1r50) and thus limits the drying of the boundary layer and the decrease of the liquid CRE (Table 5).

3.2.3 Cirrus cloud radiative effects and temperature

We separately diagnose radiative effects of clouds at temperatures below -35°C from the two MLO simulations (SEED1r50, VEL2) to evaluate the regions of highest seeding effectiveness. Both scenarios produce similar net cCRE anomalies, which follow the climatological pattern of cirrus cloudiness and their radiative impacts at the TOA, having the largest impact in the warm pool region, in storm tracks, and over orographic barriers (Fig. 6 a,b). In SEED1r50 the anomaly pattern shows an even more pronounced impact over mountain regions and the tropical warm pool than in VEL2, corresponding to regions dominated by homogeneously nucleated IC (Gasparini and Lohmann, 2016).

Temperature anomalies in general follow the anomalies in cCRE and are about 30-40% larger over land than over the ocean (Fig. 6 d,e). Moreover, both scenarios have larger responses in high latitudes, with a cooling of almost 2°C in the annual average, similar to findings of Storelvmo et al. (2014) and Muri et al. (2014). The globally average surface temperature decrease is about 30% larger in VEL2 (-0.68 $\pm$ 0.13°C) compared with SEED1r50 (-0.49 $\pm$ 0.09 °C). The difference is likely explained

Atmos. Chem. Phys. Discuss., doi:10.5194/acp-2016-1109, 2016
Manuscript under review for journal Atmos. Chem. Phys.
Published: 14 December 2016

by the larger surface forcing in VEL2 compared to SEED1r50 (-0.86 and -0.74 W m^{-2}, respectively), which is the result of a lower altitude of the maximum diabatic cooling anomaly in VEL2 (Fig. 4t). The radiative response is further amplified by changes in precipitable water, acting primarily in the tropics (Fig. 3e), and the sea ice feedback in high latitudes (not shown).

Both cCRE and temperature anomalies have a strong seasonal cycle (Fig. 6 c,f). The cooling is particularly pronounced in the winter hemisphere, and can exceed 3°C in the Arctic or 2°C in the Antarctic winter. The high-latitude cooling is a combination of atmospheric geoengineering and the ice-albedo feedback. The two scenarios exhibit remarkably similar zonally averaged temperature responses with no significant differences.

Interestingly, the SEED1r50N scenario leads to a 0.1°C larger globally averaged surface temperature cooling effect with a similar seasonality (Fig. 7a). The SEED1r50N scenario is more effective in the tropical deep convective areas, which probably originates from differences in liquid clouds (in SEED1r50 the liquid clouds have a positive CRE anomaly, Table 5). The mid and high latitude temperature anomaly pattern likely reflects changes in extratropical interannual climate variability modes. Most notably, we observe a significant Arctic cooling and warming in the northern hemispheric midlatitudes (Fig. 7 b,c), associated with a pressure decrease over the Arctic and increase over most of the midlatitudes (not shown), resembling a positive Northern Annular Mode temperature signal (Thompson and Wallace, 2000).

3.3 Alternative modelling strategies to increased sedimentation velocity

The INP seeding setup, as opposed to the increased sedimentation velocity setup, does not allow modifications of lower lying liquid origin cirrus clouds, which are mainly dynamically controlled anvils of convective clouds (Penner et al., 2015). Such clouds most likely cannot be influenced by seeding as they are less sensitive to changes in microphysics. The temperature of the boundary between liquid origin and in situ cirrus is also latitudinally dependent: a study by Jensen et al. (2015) suggested this boundary to be rather close to -70°C in the tropics, with -50°C being more representative for the midlatitudes (Voigt et al., 2016; Wernli et al., 2016).

In order to bridge the gap between increased sedimentation velocity and seeding simulations we performed an additional simulation using a lower temperature threshold of -50°C to modify prevalently in situ formed cirrus (VELmax-50). However, a large proportion of cirrus clouds that strongly influence the global radiative budget resides in the temperature range between -35°C and -50°C. The CRE of cirrus clouds colder than -50°C is only 1.7 W m^{-2} as compared to the 4.4 W m^{-2} for all cirrus clouds according to our model (Table 3). Therefore, we need to set the sedimentation velocity of IC at temperatures lower than -50°C to the maximum allowed by the model (2 m s^{-1}) to obtain a similar, but still with -0.4°C significantly smaller globally averaged cooling effect. Simulation VELmax-50 approximately reproduces the SEED1r50 cloud cover anomaly pattern (Fig. 4 a,d,e) and upper tropospheric temperature anomalies (Fig. 4 p,s,t). However, in simulation VELmax-50 the IWC at temperatures warmer than -50°C increases substantially (Fig. 4n), leading to an increase in the ICNC and IWP (Fig. 3e). Interestingly, VELmax-50 exerts a smaller radiative flux perturbation but a fast precipitation response comparable to the one in the VEL2

Atmos. Chem. Phys. Discuss., doi:10.5194/acp-2016-1109, 2016
Manuscript under review for journal Atmos. Chem. Phys.
Published: 14 December 2016

Atmospheric Chemistry and Physics Discussions

simulation (Fig. 3 a,b). Both the large fast precipitation response and the smaller temperature decrease lead to an overall net small and not statistically significant precipitation increase in the MLO simulation setup, differently from other simulations (Fig. 3d).

We additionally performed a test, in which the IC sedimentation velocity is increased for all IC (VEL2all, see Table 1). VEL2all leads to strikingly similar radiative and precipitation responses as in the VEL2 and SEED1r50 simulations, inducing a slightly larger surface cooling effect (Fig. 3d). Interestingly, in VEL2all IWC decreases throughout the atmosphere only in the extratropics. Its tropical mid-tropospheric IWC increase is likely caused by a convective activity increase (convective precipitation increase of 1.4%), resulting in a similar RH anomaly peak at 7-10 km altitude as in the VEL2 simulation (Fig. 4 g,h). These changes in tropical convection, which lead to a large number of small IC (Gasparini and Lohmann, 2016) are also responsible for an 8% increase in ICNC despite a 6% decrease in IWP. Yet, VEL2all cannot reproduce the same magnitude of cloud cover and temperature changes induced by seeding with effective INP. Our simulations show that idealised cirrus seeding by means of increased sedimentation velocity are not a good proxy for cloud macro- and microphysical changes. Nevertheless, simulations with increased IC sedimentation velocities can still provide useful information on some climatic responses (e.g. surface temperature, precipitation) to cirrus seeding.

4 Conclusions

We studied the climatic responses to cirrus seeding and to increased sedimentation velocity of ice crystals in cirrus clouds. In general, the increased sedimentation velocity simulation (VEL2) leads to qualitatively similar responses compared to cirrus seeding with large INP (SEED1r50): a decrease in cloud cover and ice water content at cirrus levels, and a temperature decrease throughout the troposphere. Ice cloud radiative effects and temperature responses are larger over land than over oceans. The pattern is particularly pronounced in the simulation SEED1r50.

The mean climatic responses of both the SEED1r50 and VEL2 simulations in terms of radiative fluxes are also similar. However, seeding by INP interacts with clouds and cloud microphysics differently compared with the increase in sedimentation velocity, implying a different atmospheric temperature response. The different vertical cooling patterns lead to a 30% larger surface temperature response in the VEL2 simulation. As the surface temperature response pattern in the annual and seasonal averages is similar, we expect to achieve the same amount of surface cooling by a smaller increase of IC sedimentation velocity. Moreover, precipitation responds to both geoengineering strategies in a similar way. The fast responses to seeding yield a $\sim$1% increase in precipitation, while the slow, temperature driven response in the mixed layer ocean simulations leads to a 0.5% decrease.

Atmos. Chem. Phys. Discuss., doi:10.5194/acp-2016-1109, 2016
Manuscript under review for journal Atmos. Chem. Phys.
Published: 14 December 2016

A large part of the cirrus induced negative CRE is counteracted by decreases in liquid clouds in the SEED1r50 simulation in response to increased convective activity. In addition, the redistribution of ice to lower levels in VEL2 leads to a positive mixed-phase cloud CRE anomaly. Our general findings indicate that increasing sedimentation velocity is a good proxy for cirrus seeding surface climate responses while it cannot reproduce the cloud macro- and microphysical responses. The additional simulations with increased sedimentation velocity for all ice crystals (VEL2all) or only for those at T<-50°C (VELmax-50) also cannot reproduce all the seeding signals from the seeding scenario. An accurate evaluation of atmospheric changes of cirrus thinning therefore requires the implementation of a cirrus microphysics scheme able to simulate the competition between homogeneous and heterogeneous ice crystal nucleation.

Our work moreover shows the non-negligible positive liquid CRE response, counteracting about half of the original cirrus CRE signal. As shown in Fig. 2, implementing seeding only during night leads to a comparable cirrus CRE and net radiative anomaly signal, without any significant counteracting effect from liquid or mixed-phase clouds (Table 5). Interestingly, such a seeding strategy leads to no significant fast precipitation response and smaller changes in IWP, ICNC, LWP, and CDNC compared to SEED1r50. Despite seeding only half of the time, we obtain a slightly larger surface temperature response in its MLO simulation, and a twice larger precipitation decrease which follows more closely the temperature dependence of the Clausius-Clapeyron relation (7% precipitation decrease per 1°C cooling). SEED1r50N therefore seems to be, due to minimal climatic and microphysical responses outside the cirrus regime, our most appealing seeding simulation.

The maximum impact on TOA radiative fluxes by the increase of ice crystal sedimentation velocity is -2.2 W m^{-2}, which corresponds to about half of the cirrus CRE and half of the radiative forcing of doubling of CO_2. The maximum impact of seeding with effective INP is, on the other hand, only about -1 W m^{-2} or 20-25% of cirrus CRE, which is achieved by injecting large ice nucleating particles of 50 μm radius in the SEED1r50 simulation.

The seeding effectiveness does not only depend on the seeding INP properties, but also on the relative frequency between both the in situ and liquid origin cirrus and homogeneously vs. heterogeneously in situ formed cirrus, which may differ between the model and observations and between different models. Furthermore, the effectiveness of cirrus seeding measured in terms of radiative anomalies is highly dependent on the cirrus CRE and consequently also on model parameters that have a large effect on cirrus optical properties (e.g. inhomogeneity parameter for ice clouds).

Ice cloud radiative effects are poorly constrained by observations on the global scale and rarely explicitly diagnosed from modelling studies. We suggest to invest more resources in understanding the cirrus cloud formation mechanisms and radiative effects at high temporal resolutions in order to better constrain CRE effects. Until then, we propose to not only state the radiative impact in terms of W m^{-2} achieved by cirrus geoengineering simulations (either by injection of seeding INP or by increasing ice crystal sedimentation velocities) but also to which fraction of the total cirrus CRE this radiative anomaly corresponds.

Atmos. Chem. Phys. Discuss., doi:10.5194/acp-2016-1109, 2016
Manuscript under review for journal Atmos. Chem. Phys.
Published: 14 December 2016

Atmospheric Chemistry and Physics Discussions

5 Code availability

6 Data availability

The data from the model simulations are available from the authors upon request.

Author contributions. TEXT

Competing interests. TEXT

Disclaimer.

Acknowledgements. The simulations were performed on Daint cluster of the Swiss National Supercomputing Center (project s431) and on the Euler ETHZ computational cluster. We would like to thank David Neubauer for his valuable comments and help on technical issues. We thank Marina Dütsch, Katty Huang, and Robert David for suggesting improvements to the manuscript. The data from the model simulations are available from the authors upon request.

Atmos. Chem. Phys. Discuss., doi:10.5194/acp-2016-1109, 2016
Manuscript under review for journal Atmos. Chem. Phys.
Published: 14 December 2016

Atmospheric Chemistry and Physics Discussions

References

Chen, T., Rossow, W. B., and Zhang, Y.: Radiative Effects of Cloud-Type Variations, J. Clim., 13, 264–286, doi:10.1175/1520-0442(2000)013<0264:REOCTV>2.0.CO;2, 2000.

Clough, S. A. and Iacono, M. J.: Line-by-line calculation of atmospheric fluxes and cooling rates: 2. Application to carbon dioxide, ozone, methane, nitrous oxide and the halocarbons, J. Geophys. Res., 100, 16 519, doi:10.1029/95JD01386, 1995.

Crook, J., Jackson, L., Osprey, S., and Forster, P. M.: A comparison of temperature and precipitation responses to different Earth radiation management geoengineering schemes, J. Geophys. Res. Atmos., 120, 9352–9373, doi:10.1002/2015JD023269., 2015.

DeMott, P. J., Cziczo, D. J., Prenni, A. J., Murphy, D. M., Kreidenweis, S. M., Thomson, D. S., Borys, R., and Rogers, D. C.: Measurements of the concentration and composition of nuclei for cirrus formation., Proc. Natl. Acad. Sci. U. S. A., 100, 14 655–60, doi:10.1073/pnas.2532677100, 2003.

Futyan, J. M., Russell, J. E., and Harries, J. E.: Determining cloud forcing by cloud type from geostationary satellite data, Geophys. Res. Lett., 32, 1–4, doi:10.1029/2004GL022275, 2005.

Gasparini, B. and Lohmann, U.: Why cirrus cloud seeding cannot substantially cool the planet, J. Geophys. Res. Atmos., 121, doi:10.1002/2015JD024666, 2016.

Hartmann, D. L., Ockert-Bell, M. E., and Michelsen, M. L.: The effect of cloud type on Earth's energy balance: results for selected regions, J. Clim., 5, 1157–1171, doi:10.1175/1520-0442(1992)005<1281:TEOCTO>2.0.CO;2, 1992.

Hong, Y., Liu, G., and Li, J.-L. F.: Assessing the Radiative Effects of Global Ice Clouds Based on CloudSat and CALIPSO Measurements, J. Clim., p. In press, doi:10.1175/JCLI-D-15-0799.1, 2016.

Hoose, C. and Möhler, O.: Heterogeneous ice nucleation on atmospheric aerosols: a review of results from laboratory experiments, Atmos. Chem. Phys., 12, 9817–9854, doi:10.5194/acp-12-9817-2012, 2012.

Ickes, L., Welti, A., Hoose, C., and Lohmann, U.: Classical nucleation theory of homogeneous freezing of water: thermodynamic and kinetic parameters, Phys. Chem. Chem. Phys., 17, 5514–5537, doi:10.1039/C4CP04184D, 2015.

Jackson, L., Crook, J., and Forster, P.: An intensified hydrological cycle in the simulation of geoengineering by cirrus cloud thinning using ice crystal fall speed changes, J. Geophys. Res. Atmos., 121, 6822–6840, doi:10.1002/ 2015JD024304, 2016.

Jensen, E. J., Pfister, L., Jordan, D. E., Bui, T. V., Ueyama, R., Singh, H. B., Thornberry, T., Rollins, A. W., Gao, R.-S., Fahey, D. W., Rosenlof, K. H., Elkins, J. W., Diskin, G. S., DiGangi, J. P., Lawson, R. P., Woods, S., Atlas, E. L., Navarro Rodriguez, M. A., Wofsy, S. C., Pittman, J., Bardeen, C. G., Toon, O. B., Kindel, B. C., Newman, P. A., McGill, M. J., Hlavka, D. L., Lait, L. R., Schoeberl, M. R., Bergman, J. W., Selkirk, H. B., Alexander, M. J., Kim, J.-E., Lim, B. H., Stutz, J., and Pfeilsticker, K.: The NASA Airborne Tropical TRopopause EXperiment (ATTREX): High-Altitude Aircraft Measurements in the Tropical Western Pacific, Bull. Am. Meteorol. Soc., doi:10.1175/BAMS-D-14-00263.1, http://journals.ametsoc.org/doi/abs/10.1175/BAMS-D-14-00263.1, 2015.

Jensen, E. J., Ueyama, R., Pfister, L., Bui, T. V., Alexander, M. J., Podglajen, A., Hertzog, A., Woods, S., Lawson, R. P., Kim, J.-e., and Schoeberl, M. R.: High-frequency gravity waves and homogeneous ice nucleation in tropical tropopause layer cirrus, Geophys. Res. Lett., doi:10.1002/2016GL069426, 2016.

Kärcher, B. and Lohmann, U.: A parameterization of cirrus cloud formation: Homogeneous freezing including effects of aerosol size, J. Geophys. Res. Atmos., 107, doi:10.1029/2001JD001429, 2002.

Kärcher, B. and Ström, J.: The roles of dynamical variability and aerosols in cirrus cloud formation, Atmos. Chem. Phys., 3, 823–838, doi:10.5194/acp-3-823-2003, 2003.

Kärcher, B., Hendricks, J., and Lohmann, U.: Physically based parameterization of cirrus cloud formation for use in global atmospheric models, J. Geophys. Res., 111, D01 205, doi:10.1029/2005JD006219, 2006.

Kienast-Sjögren, E., Rolf, C., Seifert, P., Krieger, U. K., Luo, B. P., Krämer, M., and Peter, T.: Radiative properties of mid-latitude cirrus clouds derived by automatic evaluation of lidar measurements, Atmos. Chem. Phys., 16, 7605–7621, doi:10.5194/acp-2016-32, 2016.

Köhler, C. and Seifert, A.: Identifying sensitivities for cirrus modelling using a two-moment two-mode bulk microphysics scheme, Tellus B, 67, 2015.

Kravitz, B., Robock, A., Tilmes, S., Boucher, O., English, J. M., Irvine, P. J., Jones, A., Lawrence, M. G., MacCracken, M., Muri, H., Moore, J. C., Niemeier, U., Phipps, S. J., Sillmann, J., Storelvmo, T., Wang, H., and Watanabe, S.: The Geoengineering Model Intercomparison Project Phase 6 (GeoMIP6): simulation design and preliminary results, Geosci. Model Dev., 8, 3379–3392, doi:10.5194/gmdd-8-4697-2015, 2015.

Kuebbeler, M., Lohmann, U., Hendricks, J., and Kärcher, B.: Dust ice nuclei effects on cirrus clouds, Atmos. Chem. Phys., 14, 3027–3046, doi:10.5194/acp-14-3027-2014, http://www.atmos-chem-phys.net/14/3027/2014/, 2014.

Levkov, L., Rockel, B., Kapitza, H., and Raschke, E.: 3D mesoscale numerical studies of cirrus and stratus clouds by their time and space evolution, Contrib. to Atmos. Phys., 65, 35–58, 1992.

Lohmann, U., Stier, P., Hoose, C., Ferrachat, S., Kloster, S., Roeckner, E., and Zhang, J.: Cloud microphysics and aerosol indirect effects in the global climate model ECHAM5-HAM, Atmos. Chem. Phys., 7, 3425–3446, doi:10.5194/acp-7-3425-2007, 2007.

Lohmann, U., Spichtinger, P., Jess, S., Peter, T., and Smit, H.: Cirrus cloud formation and ice supersaturated regions in a global climate model, Environ. Res. Lett., 3, 045 022, doi:10.1088/1748-9326/3/4/045022, 2008.

Luebke, A. E., Afchine, A., Costa, A., Meyer, J., Rolf, C., and Spelten, N.: The origin of midlatitude ice clouds and the resulting influence on their microphysical properties, Atmos. Chem. Phys., 16, 5793–5809, doi:10.5194/acpd-15-34243-2015, 2016.

Mitchell, D. L. and Finnegan, W.: Modification of cirrus clouds to reduce global warming, Environ. Res. Lett., 4, 045 102, doi:10.1088/1748-9326/4/4/045102, 2009.

Möhler, O., Field, P. R., Connolly, P., Benz, S., Saathoff, H., Schnaiter, M., Wagner, R., Cotton, R., Mangold, A., Heymsfield, A. J., and Karlsruhe, F.: Efficiency of the deposition mode ice nucleation on mineral dust particles, Atmos. Chem. Phys., 6, 3007–3021, 2006.

Möhler, O., Benz, S., Saathoff, H., Schnaiter, M., Wagner, R., Schneider, J., Walter, S., Ebert, V., and Wagner, S.: The effect of organic coating on the heterogeneous ice nucleation efficiency of mineral dust aerosols, Environ. Res. Lett., 3, 025 007, doi:10.1088/1748-9326/3/2/025007, 2008.

Muri, H., Kristjánsson, J. E., Storelvmo, T., and Pfeffer, M. a.: The climatic effects of modifying cirrus clouds in a climate, J. Geophys. Res. Atmos., 119, 4174–4191, doi:10.1002/2013JD021063., 2014.

Neubauer, D., Lohmann, U., Hoose, C., and Frontoso, M. G.: Impact of the representation of marine stratocumulus clouds on the anthropogenic aerosol effect, Atmos. Chem. Phys., 14, 11 997–12 022, doi:10.5194/acpd-14-13681-2014, 2014.

Nordeng, T. E.: Extended versions of the convective parametrization scheme at ECMWF and their impact on the mean and transient activity of the model in the tropics, Tech. rep., ECMWF, 1994.

Penner, J. E., Zhou, C., and Liu, X.: Can cirrus cloud seeding be used for geoengineering?, Geophys. Res. Lett., 42, 8775–8782, doi:10.1002/2015GL065992, 2015.

Rieck, M., Nuijens, L., and Stevens, B.: Marine Boundary Layer Cloud Feedbacks in a Constant Relative Humidity Atmosphere, J. Atmos. Sci., 69, 2538–2550, doi:10.1175/JAS-D-11-0203.1, 2012.

Sherwood, S. C., Bony, S., and Dufresne, J.-L.: Spread in model climate sensitivity traced to atmospheric convective mixing., Nature, 505, 37–42, doi:10.1038/nature12829, 2014.

Spichtinger, P. and Gierens, K. M.: Modelling of cirrus clouds – Part 1a: Model description and validation, Atmos. Chem. Phys., 9, 685–706, doi:10.5194/acp-9-685-2009, 2009.

Stevens, B., Giorgetta, M., Esch, M., Mauritsen, T., Crueger, T., Rast, S., Salzmann, M., Schmidt, H., Bader, J., Block, K., Brokopf, R., Fast, I., Kinne, S., Kornblueh, L., Lohmann, U., Pincus, R., Reichler, T., and Roeckner, E.: Atmospheric component of the MPI-M Earth System Model: ECHAM6, J. Adv. Model. Earth Syst., 5, 146–172, doi:10.1002/jame.20015, 2013.

Stier, P., Feichter, J., Kinne, S., Kloster, S., Vignati, E., Wilson, J., Ganzeveld, L., Tegen, I., and Werner, M.: The aerosol-climate model ECHAM5-HAM, Atmos. Chem. Phys., pp. 1125–1156, 2005.

Stocker, T.F., D. Qin, G.-K. Plattner, L.V. Alexander, S.K. Allen, N.L. Bindoff, F.-M. Bréon, J.A. Church, U. C., S. Emori, P. Forster, P. Friedlingstein, N. Gillett, J.M. Gregory, D.L. Hartmann, E. Jansen, B. Kirtman, R. Knutti, K., Krishna Kumar, P. Lemke, J. Marotzke, V. Masson-Delmotte, G.A. Meehl, I.I. Mokhov, S. Piao, V. Ramaswamy, D., Randall, M. Rhein, M. Rojas, C. Sabine, D. Shindell, L.D. Talley, D. V., and Xie, S.-P.: IPCC AR5: Technical Summary, Tech. rep., 2013.

Storelvmo, T. and Herger, N.: Cirrus cloud susceptibility to the injection of ice nuclei in the upper troposphere, J. Geophys. Res. Atmos., 119, 2375–2389, doi:10.1002/2013JD020816, 2014.

Storelvmo, T., Boos, W. R., and Herger, N.: Cirrus cloud seeding: a climate engineering mechanism with reduced side effects?, Philos. Trans. R. Soc. A Math. Phys. Eng. Sci., 372, 20140 116–20140 116, doi:10.1098/rsta.2014.0116, 2014.

Thompson, D. W. J. and Wallace, J. M.: Annular Mode in the Extratropical Circulation. Part I : Month-to-Month Variability, J. Clim., 13, 1000–1016, doi:http://dx.doi.org/10.1175/1520-0442(2000)013<1000:AMITEC>2.0.CO;2, 2000.

Tiedtke, M.: A comprehensive mass flux scheme for cumulus parameterization in large-scale models, doi:10.1175/1520-0493(1989)117<1779:ACMFSF>2.0.CO;2, 1989.

Vignati, E., Wilson, J., and Stier, P.: M7: An efficient size-resolved aerosol microphysics module for large-scale aerosol transport models, J. Geophys. Res. D Atmos., 109, 1–17, doi:10.1029/2003JD004485, 2004.

Voigt, C., Schumann, U., Minikin, A., Abdelmonem, A., Afchine, A., Borrmann, S., Boettcher, M., Buchholz, B., Bugliaro, L., Costa, A., Curtius, J., Dollner, M., Dörnbrack, A., Dreiling, V., Ebert, V., Ehrlich, A., Fix, A., Forster, L., Frank, F., Fütterer, D., Giez, A., Graf, K., Grooß, J.-U., Groß, S., Heimerl, K., Heinold, B., Hüneke, T., Järvinen, E., Jurkat, T., Kaufmann, S., Kenntner, M., Klingebiel, M., Klimach, T., Kohl, R., Krämer, M., Candra Krisna, T., Luebke, A., Mayer, B., Mertes, S., Molleker, S., Petzold, A., Pfeilsticker, K., Port, M., Rapp, M., Reutter, P., Rolf, C., Rose, D., Sauer, D., Schäfler, A., Schlage, R., Schnaiter, M., Schneider, J., Spelten, N., Spichtinger, P., Stock, P., Walser, A., Weigel, R., Weinzierl, B., Wendisch, M., Werner, F., Wernli, H., Wirth, M., Zahn, A., Ziereis, H., and Zöger, M.: ML-CIRRUS - The airborne experiment on natural cirrus and contrail cirrus with the high-altitude long-range research aircraft HALO, Bull. Am. Meteorol. Soc., pp. BAMS–D–15–00 213.1, doi:10.1175/BAMS-D-15-00213.1, 2016.

Wernli, H., Boettcher, M., Joos, H., Miltenberger, A. K., and Spichtinger, P.: A trajectory-based classification of ERA-Interim ice clouds in the region of the North Atlantic storm track, Geophys. Res. Lett., 43, 1–8, doi:10.1002/2016GL068922.1., 2016.

Zhang, K., O'Donnell, D., Kazil, J., Stier, P., Kinne, S., Lohmann, U., Ferrachat, S., Croft, B., Quaas, J., Wan, H., Rast, S., and Feichter, J.: The global aerosol-climate model ECHAM-HAM, version 2: sensitivity to improvements in process representations, Atmos. Chem. Phys., 12, 8911–8949, doi:10.5194/acp-12-8911-2012, 2012.

Atmos. Chem. Phys. Discuss., doi:10.5194/acp-2016-1109, 2016
Manuscript under review for journal Atmos. Chem. Phys.
Published: 14 December 2016

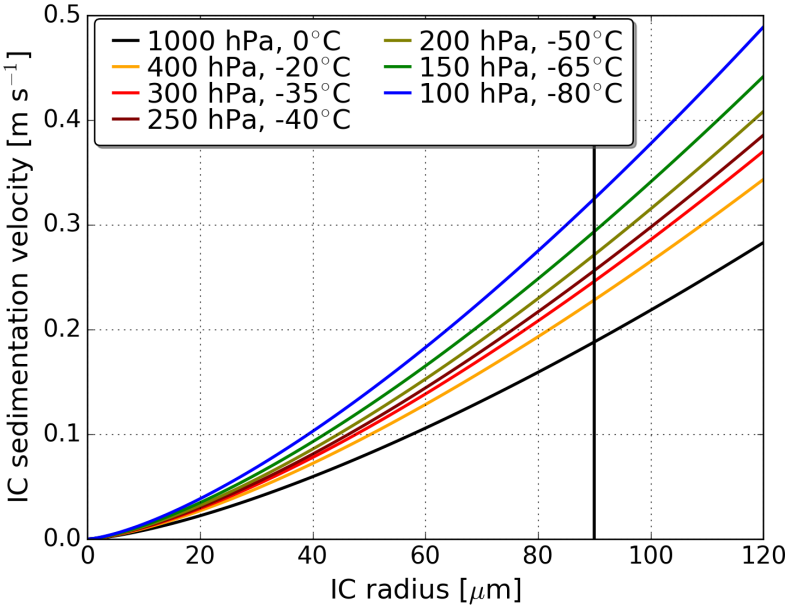

Figure 1. Ice crystal sedimentation velocities as a function of IC radius for the selected atmospherically relevant conditions in ECHAM-HAM (Spichtinger and Gierens, 2009). The black vertical line represents the maximum radius ice crystals can have before they are transferred to the precipitating snow category.

Atmos. Chem. Phys. Discuss., doi:10.5194/acp-2016-1109, 2016
Manuscript under review for journal Atmos. Chem. Phys.
Published: 14 December 2016

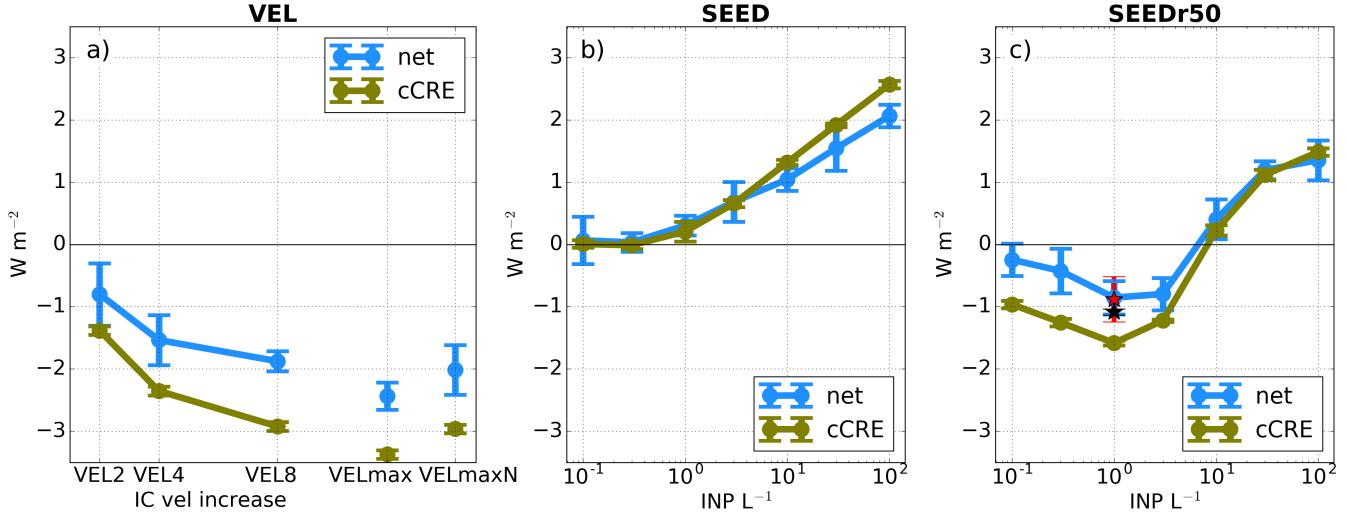

Figure 2. 5-year TOA anomalies of net radiative fluxes (NET) and net cirrus cloud radiative effects (cirrus CRE) for fixed SST simulations of seeding with increased sedimentation velocities (a). b) shows net radiative fluxes and cirrus CRE for seeding simulations with different 0.5 μm sized INP, while c) shows the equivalent for seeding with 50 μm INP. The stars in c) show results from the SEED1r50N simulation with seeding performed only at night where the red star represents the net anomalies and black one cirrus CRE anomalies. The error bars represent $\pm$ 2 standard deviations.

Atmos. Chem. Phys. Discuss., doi:10.5194/acp-2016-1109, 2016
Manuscript under review for journal Atmos. Chem. Phys.
Published: 14 December 2016

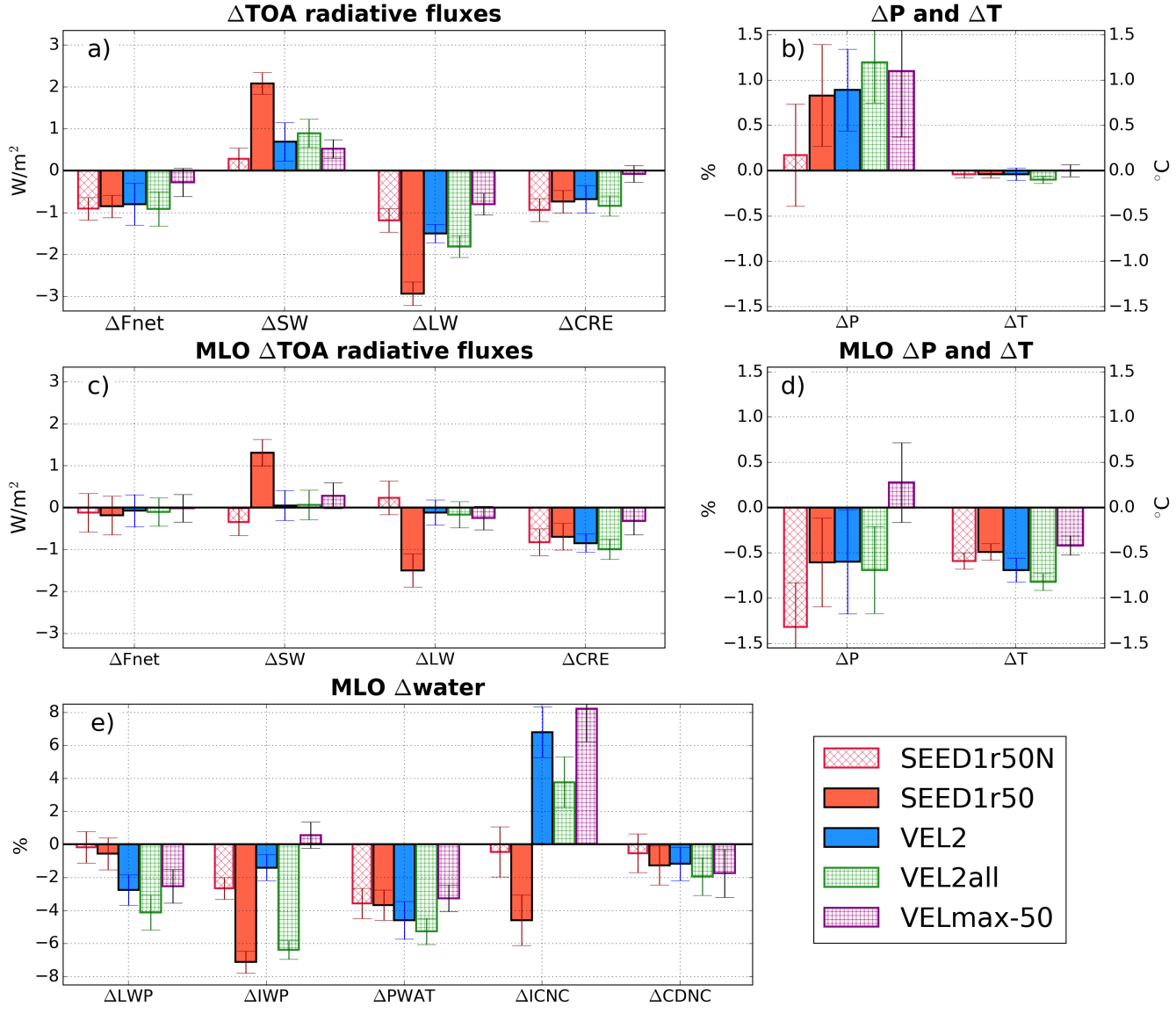

Figure 3. Annually averaged anomalies for top-of-the-atmosphere (TOA) energy fluxes (a,c), and precipitation (P), temperature (T) (b,d) and the selected microphysical quantities (e): liquid water path (LWP), ice water path (IWP), precipitable water (PWAT), ice crystal number concentration (ICNC), cloud droplet number concentration (CDNC). a) and b) show anomalies of fixed SST simulations, c), d), and e) are from mixed layer ocean (MLO) simulations. The error bars represent the ± 2 standard deviation range.

Atmos. Chem. Phys. Discuss., doi:10.5194/acp-2016-1109, 2016
Manuscript under review for journal Atmos. Chem. Phys.
Published: 14 December 2016

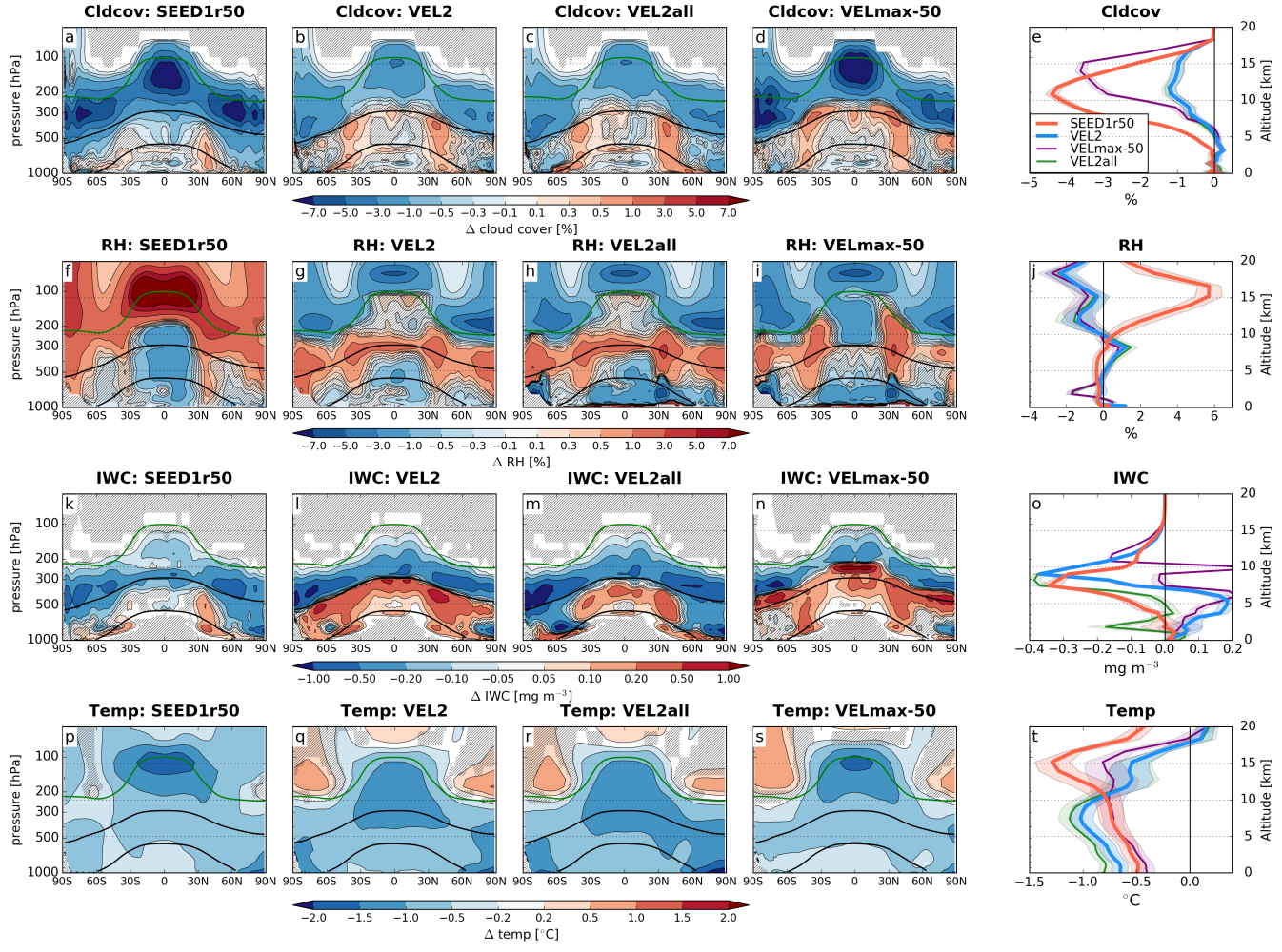

Figure 4. Annually averaged anomalies of cloud cover (Cldcov, a-e), relative humidity with respect to liquid water (RH, f-j), ice water content (IWC, k-o), and temperature (Temp, p-t) for SEED1r50 and VEL2 MLO simulations (see Table 1). The green curve represents the tropopause, while the black curves are the -35°C and the 0°C isolines. The hatching is applied for anomalies not significant at the 95% confidence level. On the right hand the anomalies are averaged over latitude and longitude.

Atmos. Chem. Phys. Discuss., doi:10.5194/acp-2016-1109, 2016
Manuscript under review for journal Atmos. Chem. Phys.
Published: 14 December 2016

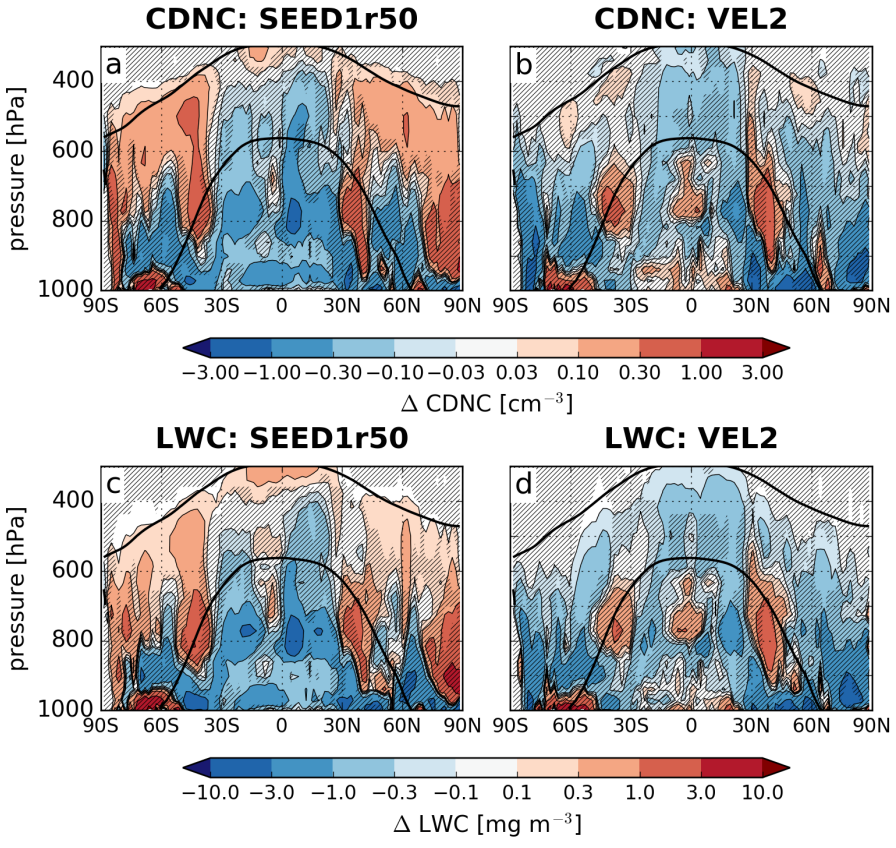

Figure 5. Annually averaged anomalies of the cloud droplet number concentration (CDNC, a,b) and liquid water content (LWC, c,d) for SEED1r50 and VEL2 fixed SST simulations (see Table 1). The black curves are the -35°C and the 0°C isolines. The hatching is applied for anomalies not significant at the 95% confidence level.

Atmos. Chem. Phys. Discuss., doi:10.5194/acp-2016-1109, 2016
Manuscript under review for journal Atmos. Chem. Phys.
Published: 14 December 2016

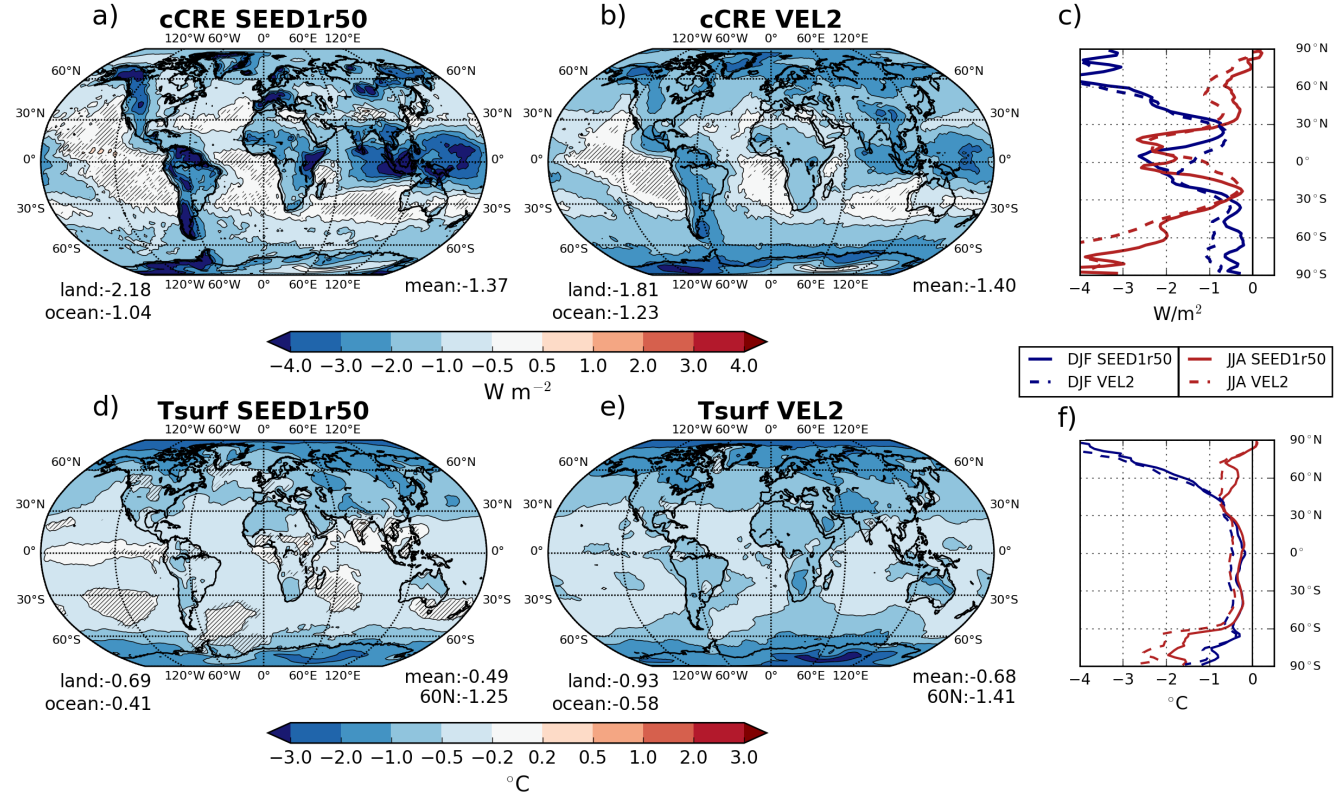

Figure 6. Annually averaged anomalies of cirrus cloud radiative effect (cCRE, a,b) and surface temperature (Tsurf, c,d) from the SEED1r50 and VEL2 MLO simulations. The hatching is applied for anomalies not significant at the 95% confidence level. Panels c) and f) show the respective annual zonal averages for DJF (blue) and JJA (red).

Atmos. Chem. Phys. Discuss., doi:10.5194/acp-2016-1109, 2016
Manuscript under review for journal Atmos. Chem. Phys.
Published: 14 December 2016

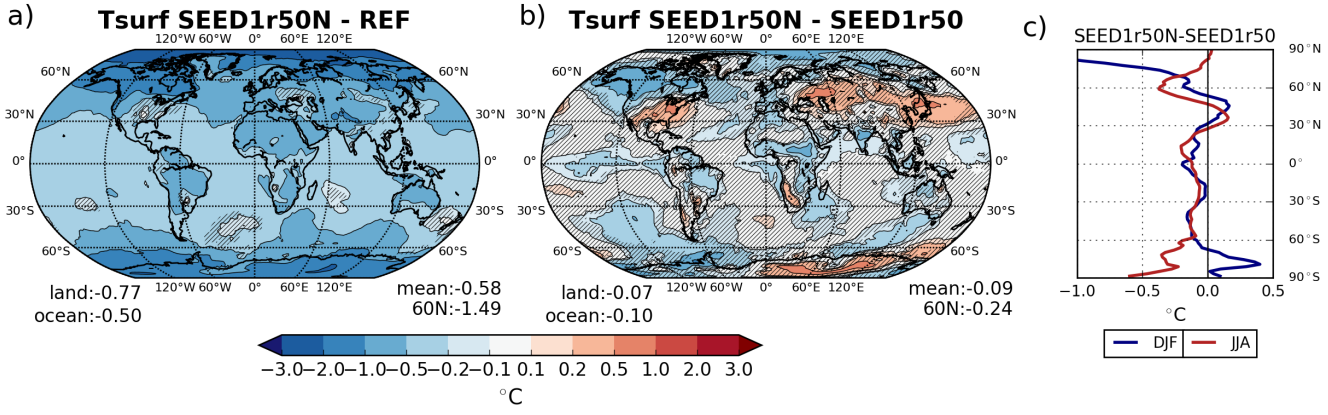

Figure 7. Annually averaged anomalies of surface temperature (Tsurf) for the SEED1r50N simulation plotted in anomaly with respect to REF (a) or SEED1r50 (b). The hatching is applied for anomalies not significant at the 95% confidence level. Panel c) shows the respective annual zonal average anomalies of SEED1r50N with respect to SEED1r50 for DJF (blue) and JJA (red). All simulations are performed in the MLO setup.

Atmos. Chem. Phys. Discuss., doi:10.5194/acp-2016-1109, 2016
Manuscript under review for journal Atmos. Chem. Phys.
Published: 14 December 2016

Atmospheric Chemistry and Physics Discussions

Table 1. Simulation terminology and their respective cirrus geoengineering method.

Simulation	Sim. length [y]	IC sedimentation	seed INP conc. [L^{-1}]	seed INP radius [μm]
fixed SST				
REF	10	/	/	/
VEL2	10	2 x ref	/	/
VEL4	5	4 x ref	/	/
VEL8	5	8 x ref	/	/
VELmax	5	set to 2 m/s	/	/
VELmaxN	5	set to 2 m/s at night	/	/
VEL2all	5	2 x ref (all IC)	/	/
VELmax-50	5	2 x ref (at T<-50°C)	/	/
SEED0.1	5	/	0.1	0.5
SEED0.3	5	/	0.3	0.5
SEED1	5	/	1	0.5
SEED3	5	/	3	0.5
SEED10	5	/	10	0.5
SEED30	5	/	30	0.5
SEED100	5	/	100	0.5
SEED0.1r50	5	/	0.1	50
SEED0.3r50	5	/	0.3	50
SEED1r50	10	/	1	50
SEED3r50	5	/	3	50
SEED10r50	5	/	10	50
SEED30r50	5	/	30	50
SEED100r50	5	/	100	50
SEED1r50N	10	/	1 at night	50
SEED1r5	5	/	1	5
SEED1r10	5	/	1	10
SEED1r20	5	/	1	20
MLO				
REF	50	/	/	/
SEED1r50	50	/	1	50
SEED1r50N	50	/	1 at night	50
VEL2	50	2 x ref	/	/
VEL2all	50	2 x ref (all IC)	/	/
VELmax-50	50	2 x ref (at T<-50°C)	/	/

Atmos. Chem. Phys. Discuss., doi:10.5194/acp-2016-1109, 2016
Manuscript under review for journal Atmos. Chem. Phys.
Published: 14 December 2016

Atmospheric Chemistry and Physics Discussions

Table 2. Cirrus CRE anomalies in W m^{-2} with respect to REF (first column) or with respect to the simulation with two times smaller IC sedimentation velocities (second column) for fixed SST simulations. The last column represents the relative fraction of the cirrus cloud radiative effect (cCRE) anomaly with respect to the remaining cCRE.

	ΔcCRE [W m^{-2}]	**Δ remaining cCRE [W m^{-2}]**	**Δ remaining cCRE [%]**
VEL2	-1.43	-1.43	-33%
VEL4	-2.40	-0.97	-33%
VEL8	-2.98	-0.58	-30%

Table 3. Net cirrus cloud radiative effects (cCRE) from the fixed SST REF simulation of all clouds at temperatures colder than the one stated in the left column. The right column represents the percentage contribution to the total cCRE.

Temp [°C]	**cCRE [W m^{-2}]**	**percentage [%]**
-35	4.35	100
-40	3.42	79
-45	2.49	57
-50	1.73	40
-55	1.22	28
-60	0.83	19
-65	0.53	12
-70	0.34	8

Table 4. Top-of-the-atmosphere net radiative balance (F_{net}) anomalies in W m^{-2} for seeding with 1 INP L^{-1} with varying INP radius and the $\pm$ 2 standard deviation range for fixed SST simulations.

	SEED1	**SEED1r5**	**SEED1r10**	**SEED1r20**	**SEED1r50**
ΔF_{net} [W m^{-2}]	0.30 ± 0.30	0.01 ± 0.44	-0.03 ± 0.41	-0.46 ± 0.14	-0.85 ± 0.40

Table 5. Top-of-the-atmosphere net cloud radiative effect anomalies from cirrus clouds (cCRE, for temperatures <-35°C), mixed-phase clouds (mpCRE, -35°C < T < 0°C), and liquid clouds (liqCRE, T > 0°C) for the VEL2, SEED1r50, and SEED1r50N fixed SST simulations. The radiative anomalies are further divided into their LW and SW components (shown in parenthesis).

simulation	**ΔliqCRE** (LW, SW) [W m^{-2}]	**ΔmpCRE** (LW, SW) [W m^{-2}]	**ΔcCRE** (LW, SW) [W m^{-2}]	**ΔtotCRE** (LW, SW) [W m^{-2}]
VEL2	0.09 ± 0.38 (0.02, 0.07)	0.41 ± 0.12 (0.82, -0.42)	-1.43 ± 0.06 (-2.02, 0.60)	-0.84 ± 0.41(-1.47, 0.63)
SEED1r50	0.96 ± 0.25 (0.00, 0.96)	0.15 ± 0.10 (0.24, -0.10)	-1.63 ± 0.03 (-2.47, 0.84)	-0.82 ± 0.31 (-2.90, 2.08)
SEED1r50N	0.15 ± 0.14 (0.01, 0.14)	0.18 ± 0.18 (0.13, 0.04)	-1.06 ± 0.03 (-1.07, 0.02)	-0.95 ± 0.20 (-1.21, 0.26)